# Electrical conductivity of crack-template based transparent conductive films: A computational point of view

Yuri Yu. Tarasevich, Andrei V. Eserkepov, and Irina V. Vodolazskaya

Laboratory of Mathematical Modeling, Astrakhan State University, Astrakhan, 414056, Russia

(\*vodolazskaya\_agu@mail.ru)

(\*dantealigjery49@gmail.com)

(\*Corresponding author: tarasevich@asu.edu.ru)

(Dated: September 11, 2023)

Crack-template-based transparent conductive films (TCFs) are promising kinds of junction-free, metallic network electrodes that can be used, e.g., for transparent electromagnetic interference (EMI) shielding. Using image processing of published photos of TCFs, we have analyzed the topological and geometrical properties of such crack templates. Additionally, we analyzed the topological and geometrical properties of some computergenerated networks. We computed the electrical conductance of such networks against the number density of their cracks. Comparison of these computations with predictions of the two analytical approaches revealed the proportionality of the electrical conductance to the square root of the number density of the cracks was found, this being consistent with the theoretical predictions.

### I. INTRODUCTION

When transparent conductive films (TCFs) are used for electromagnetic interference (EMI) shielding in the optical imaging domain, uniform illumination is crucial for ensuring the imaging quality while the light beam penetrates the metal mesh. The stray light energy from high-order diffractions by the random mesh is significantly less than that from regularly structured meshes (square, honeycomb), which indicates the good optical performance of such random meshes [1–6]. In contrast to meshes with periodically aligned metal lines, random metal networks produce neither moiré nor starburst patterns; this property is crucial for their application in displays [7–11].

To characterize nanowire-based and templated transparent conductive films, the metal filling factor,  $f_{\rm F}$ , i.e., ratio of the metal-covered area to the total area of the film, is used. The metal fill factor defined in this way and the transmittance, T, are connected as follows

$$T = 1 - f_{\rm F} \tag{1}$$

(see, e.g., Lee *et al.* [12]). However, for real-world systems, this relationship is only approximately valid (see Table I).

Jiang et al. [4], Ghosh et al. [30] used the relation

$$T = (1 - f_{\rm F})^2,\tag{2}$$

which assumes an unusual definition of the filling factor, viz., for a regular square grid,

$$f_{\rm F} = \frac{w}{G + w},\tag{3}$$

where w is the line width, while G is the grid spacing defined as the shortest distance between two parallel conductive lines (not their pitch!) [30]. Hence,

$$T = \left(\frac{G}{G+w}\right)^2,\tag{4}$$

This relation has also been used for regular grids of other structures and for irregular meshes [4]. For a regular square

metallic grid, Schneider et al. [31] estimated the transmittance as follows

$$T = 1 - f_{\rm F} = \left(\frac{p - w}{p}\right)^2,\tag{5}$$

where p is the pitch. Since p = G + w (see Fig. 1), the transparencies (4) and (5) are identical.

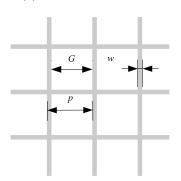


FIG. 1. Main sizes used in definitions of the filling factor and of transparency. Here, p is the pitch, w is the line width, G is the grid spacing.

For a regular, square grid, the sheet resistance depends on the fill factor as follows

$$R_{\square} = \xi \frac{\rho}{t f_{\rm F}},\tag{6}$$

where  $\rho$  is the electrical resistivity of the material, t is the thickness of the lines, and  $\xi$  is the correction factor [30, 31]. Accounting for (5) and (6),

$$T = 1 - \xi \frac{\rho}{tR_{\square}}. (7)$$

By contrast, Muzzillo *et al.* [32], assuming the grids had an idealized square shape, used a quadratic dependence of the transparency on the inverse sheet resistance (i.e., the sheet conductance)

$$T = \left(1 - \frac{B\rho}{tR_{\square}}\right)^2,\tag{8}$$

1.1222 1.11 cannot be of the contract of the c								
Source	Metal	Substrate	$R_{\square},\Omega/\square$	T,%	$f_{\mathrm{F}}$ , %	w, µm	t, nm	pitch, $\mu$ m
Rao and Kulkarni [13]	Au	quartz	5.4	87	20	2	60	20
Rao and Kulkarni [13]	Au	quartz	3.1	87	20	2	220	20
Han <i>et al</i> . [14]	Ag	glass	4.2	82	8.4	2	60	45
Han <i>et al</i> . [14]	Ag	PET <sup>a</sup>	10	88	8.4	1	60	65
Han <i>et al</i> . [2]	Ag	quartz		91		0.5-2	200	30-80
Rao <i>et al</i> . [15]	Ag	glass	10	86	20	2	55	20-60
Pei <i>et al</i> . [16]	Ag	glass	6.8	86	14	2	50	20-80
Peng <i>et al</i> . [17]	Ag	PET	3.7-39.6	88.0-99.4	0.21-10.25	0.5 - 5	10-150	40-470
Voronin et al. [18]	Ag	PET	21.4	91.6		$14 \pm 0.5$	70	$78.7 \pm 25.2$
Voronin et al. [18]	Ag	PET	12.3	90.1		$14 \pm 0.5$	140	$78.7 \pm 25.2$
Voronin et al. [18]	Ag	PET	8.1	87.4		$14 \pm 0.5$	210	$78.7 \pm 25.2$
Voronin et al. [19]	Ag	PET	1.3	77.3	< 20	2.4-18.8	300	40.1-97.5
Voronin et al. [19]	Ag	PET	4.1	85.7	< 20	2.4-18.8	300	40.1-97.5
Voronin et al. [20]	Ag	PET	11.2	90.2	10.2	$3.3 \pm 0.8$	200	$63 \pm 22$
Voronin et al. [20]	Ag	PET	6.8	83.6	15.5	$5.4 \pm 1.4$	200	$67 \pm 25$
Voronin et al. [21]	Ag	PET	11	89.8	9.8	4.7	109	50
Voronin et al. [22]	Ag	PET	1.59	89.1	2.9-17	1.2-6.2	600-2500	59.76-94.23
Kang et al. [23]	Ag	PET	1.01-5.7	88-91.8		0.85 - 1.53	350-750	15.0-22.96
Cheuk et al. [24]	Ag	glass	7.8 - 32.0	82	9.04-36.8	6.6-21.6	100	55-137 <sup>b</sup>
Voronin et al. [25]	Cu	PET, glass	2.43	91.2	7.85	$7.05 \pm 1.77$	$443.14 \pm 19.75$	$177.5 \pm 72.9$
Voronin et al. [25]	Cu	PET, glass	0.53	73.8	19.5	$7.87 \pm 1.09$	$723.03 \pm 50.15$	$76.5 \pm 35.5$
Walia <i>et al</i> . [10]	Cu	PET	0.79	90	12.5		300	
Walia <i>et al</i> . [26]	Cu	PET	0.83 - 1000	77.6–95	7.5–25	4.5-10	20-1000	15-35
Liu <i>et al</i> . [27]	Cu	PET	3.4-13.4	76.5–93		1.5	120	
Mondal et al. [28]	Al	glass	6	91.5	9	10	400	100
Govind et al. [29]	Al	PET	6.42–55	85–95		3–20	140–200	

TABLE I. A summary of experimental data on crack-template-based transparent conductive films.

where B is the fitting constant.

For irregular metal meshes based on cracked templates, Voronin *et al.* [25] defined the fill factor as follows

$$f_{\rm F} = 1 - \left(\frac{g - w}{g}\right)^2,\tag{9}$$

where g is the average cell size, while w is the average crack width. Hence, the transmittance is equal to

$$T = \left(\frac{g - w}{g}\right)^2. \tag{10}$$

Using geometrical considerations, Kumar and Kulkarni [33] evaluated the sheet resistances of random metallic networks as

$$R_{\square} = \frac{\pi \rho}{2wt\sqrt{n_{\rm E}}},\tag{11}$$

where  $\rho$  is the resistivity of the material, w and t are the width and the thickness of the rectangular wire, respectively, and  $n_{\rm E}$  is the number of wire segments per unit area. According to Kumar and Kulkarni [33], in a sample  $L_x \times L_y$ , the number of cracks intersecting an equipotential line is

$$N_{x} = \sqrt{n_{\rm E}} L_{\rm v},\tag{12a}$$

$$N_{y} = \sqrt{n_{\rm E}} L_{x},\tag{12b}$$

when the potential difference,  $U_0$ , is applied along the x- or y-axis, respectively. The current distribution has also been calculated in conducting crack-template-based metallic networks [34].

A similar approach has been applied to anisotropic systems [35]. In this case, the sheet resistance can be written as

$$R_{\square} = \frac{2\rho}{wtn_{\rm E}\langle l\rangle(1\pm s)},\tag{13}$$

where l is the length of the crack segment, hereinafter  $\langle \cdot \rangle$  denotes an average value,

$$s = 2\langle \cos^2 \theta \rangle - 1 \tag{14}$$

is the orientational order parameter [36], and  $\theta$  is the angle between a wire and the *x*-axis. For isotropic systems (s = 0), equations (11) and (13) differ since they are based on different assumptions regarding the number of wires intersecting a line. According to Tarasevich *et al.* [35], the number of cracks intersecting an equipotential line is

$$N_x = \frac{2\langle l \rangle n_{\rm E} L_y}{\pi},\tag{15a}$$

$$N_{y} = \frac{2\langle l \rangle n_{\rm E} L_{x}}{\pi}.$$
 (15b)

<sup>&</sup>lt;sup>a</sup> Polyethylene terephthalate

<sup>&</sup>lt;sup>b</sup> Computed as square root of the cell area.

The average length of the crack segments is expected to be dependent on the number density of the cracks as

$$\langle l \rangle = \beta n_{\rm E}^{-1/2}.\tag{16}$$

This relation can be easily checked (not proved!) using, e.g., a regular square mesh. The factor  $\beta$  depends on the shape factor (circularity) of the cells

$$C = \frac{4\pi A}{P^2},\tag{17}$$

where *A* is the cell area and *P* is the cell perimeter.

The crack density is defined as the total crack length,  $L_c$ , divided by the area of the reference surface, A [37],

$$\rho_{\rm c} = \frac{L_c}{A}.\tag{18}$$

In general terms, omitting technical details, the manufacture of crack-template-based TCFs consists of the following steps. A treated substrate (glass, quartz, PET, etc.) is covered (using, e.g., the Meyer rod method or by spin coating) width a thin film of a polymer or colloid (e.g., egg white). This thin film cracks due to desiccation, producing a crack template. A metal (Au, Ag, Cu, Al, etc.) is sputtered onto the template. Then, the template may be removed (e.g., dissolved). The metal mesh on the substrate is used as a seed for the galvanic deposition of the same or another metal. Although the actual technology may differ significantly, this description offers a basic idea of the manufacture of crack-template-based TCFs. Detailed descriptions of the manufacturing of each particular sample can be found in the appropriate references presented in Table I.

Basic information regarding the formation and modelling of desiccation crack patterns can be found in Goehring et al. [38]. Zeng et al. [39] proposed a coupled electrothermal model to describe the physical properties of crack-templatebased transparent conductive films. The geometry of the random metallic network was generated by applying a Voronoi diagram. In particular, the current density and heating power have been computed using COMSOL. Kim and Truskett [40] proposed a geometric modeling approach for crack-templatebased networks. The authors mimicked real-world crack patterns using a Voronoi tessellation. Within Model I, wires of varying width were assigned to the edges of the polygonal cells of the Voronoi tessellation. The resulting geometry in Model I is hyperuniform. Within Model II, wires of equal width were assigned to the edge of each Voronoi polygon. The authors computed the optical transmittance and the sheet resistance of these networks. In fact, both these models use an assumption that the width of the cracks was distributed independently and they ignored the hierarchy of the cracks. However, the widths of the any adjacent segments of the same crack are not independent; besides, primary cracks are wider than secondary ones. Nevertheless, when the mean electrical properties are of interest, the fine structure of any particular crack pattern might effectively be negligible. This issue needs to be additionally studied, at least. Esteki et al. [41] mimicked seamless metallic nanowire networks using a Voronoi tessellation. A computational study of the thermo-electrooptical properties of these networks and their geometrical features was performed using in-house computational implementations and a coupled electrothermal model built in COMSOL Multiphysics software.

Although an extensive comparison of real-world crack patterns and mosaics (Gilbert and Voronoi tessellations) has recently been performed [42], we have applied a simpler analysis to find some common features of the crack patterns used in TCE production.

The goal of the present work is an investigation of the topological, geometrical and electrical properties of TCFs obtained using crack templates, as well as of artificial computergenerated networks that are intended to mimic the properties of interest of these real-world TCFs.

The rest of the paper is constructed as follows. Section II describes technical details of the image processing and simulation, together with the analytical approach, but also presents some preliminary results. Section III presents our main findings. Section IV summarizes the main results. Some mathematical details are presented in Appendix A, Appendix B, and Appendix C.

# II. METHODS

## A. Sampling

We studied 10 real crack-template-based networks and two kinds of computer-generated networks. We refer to the real-world networks as sample 1 and sample 2, and these correspond to the samples[43] described in Ref. 21, while sample 3 corresponds to Voronin *et al.* [18, cropped Fig. 2(a)]; sample 4, which corresponds to Xian *et al.* [44, cropped Fig. 2(a)], while sample 5, sample 6, and sample 7 correspond to Gao *et al.* [45, Fig. 2, cropped subfigures (a), (b), and (c), correspondingly]; sample 8, sample 9, and sample 10 correspond to Pei *et al.* [16, Fig. 2, cropped subfigures (a), (b), and (c), respectively].

Table I shows that there is a significant spread in materials and parameters used; in the available literature, the values of sheet resistances are not always related to specific values of geometric parameters, while in cases where photographs of the samples are given, their specific electrical and geometric characteristics are often missing. For these reasons, we are unable directly to compare the results of our computations with available experimental data. Instead, for analysis, we have used the reduced electrical conductance.

We refer to the computer-generated networks as Voronoi and VoronoiHU. Figure 2(b) and fig. 2(c) demonstrate examples of such computer-generated networks. These networks were produced by applying the Voronoi tessellation in MAT-LAB. In the first case, the points were randomly distributed within a square domain. In the second case, discs were deposited in the square domain using random sequential adsorption. The centers of these discs were used as random hyperuniformly distributed points in order to perform a Voronoi tessellation. Note, that the VoronoiHU networks resemble

printed random meshes[1, 3, 6] rather than crack-template-based networks.

### B. Image processing

To process the images of crack patterns, we used StructuralGT, a Python package for automated graph theory analvsis of structural network images [46]. StructuralGT was modified to match our particular requirements. Figure 2(a) demonstrates an example of a crack pattern along with its corresponding network. This network, which mimics the crack pattern, was generated using StructuralGT [46]. The sample size is  $1.65 \times 1.2365$  mm. The network of this particular crack pattern contains 899 nodes and 1249 edges. The average degree is  $\deg V \approx 2.78$ . Nodes with  $\deg V = 1$  correspond to dead ends as well as to the intersections of edges with the domain boundaries, while ones with  $\deg V = 2$  correspond to bent cracks. The overall length of edges, which are incident on nodes with  $\deg V = 1$ , is about 7.4% of the total length of edges. Analysis of the crack widths was omitted due to the modest resolution of the images, which would have lead to insufficient accuracy.

### C. Computational details

The networks under consideration (both the real-world samples and computer-generated networks) were treated as random resistor networks (RRNs), where each network edge corresponded to a resistor, while each node corresponded to a junction between resistors. The resistance of an *i*-th resistor can be written as

$$R_i = \rho \frac{l_i}{A_i},\tag{19}$$

where  $l_i$  is the crack length, while  $A_i = w_i t_i$  is the area of the cross-section of the metal that fills the crack. We supposed that all such metal wires have the same width and thickness. The impact of variable width of a conductor on the electrical resistance is considered in Appendix A.

We attached a pair of superconducting buses to the two opposite boundaries of the systems in such a way, that the potential difference,  $U_0$ , was applied either along axis x or along axis y. Applying Ohm's law to each resistor and Kirchhoff's point rule to each junction, a system of linear equations (SLEs) was obtained. The matrix of this SLE is sparse. Such an SLE can be solved numerically to find the potentials and currents in the RRN under consideration. We used the EIGEN library[47] to solve the SLEs. In particular, our computations evidenced that the potential drop along the samples is close to linear (Fig. 3). When the current in each resistor is known, the total electric current can be calculated. Since the applied potential difference,  $U_0$ , is known, the total resistance and the conductance of the RRN can be found using Ohm's law. We use subscripts x and y to distinguish the resistances and conductances along axis x or along axis y. Then, the sheet resistance and conductance could be found, since

$$R_{\square} = R_x \frac{L_y}{L_x} = R_y \frac{L_x}{L_y}.$$
 (20)

## D. Theoretical description

A geometrical consideration has been used to evaluate the electrical conductivity of crack-template-based TCFs [33]. In fact, this consideration is a kind of mean-field approach, since a single wire (crack segment) is considered to be placed in a homogeneous electric field produced by all the other wires. In our study, we used a very similar idea and treated as crack-template-based TCFs as random networks.

Since homogeneous cracking structures without clusters and blind cracks (dead ends) can be produced [18, 21], we suppose that

- 1. the template consists of a single cluster, i.e., there is only one connected component in the corresponding network;
- 2. there are no dead ends, i.e.,  $\deg V > 1$  for any node in the corresponding network;
- 3. the crack template is isotropic, i.e., all crack orientations are equiprobable.

These assumptions will be validated in Section III using a computer simulation.

The sheet resistance is

$$R_{\square} = \frac{2\rho}{n_{\rm E}\langle l\rangle_{W}t}.\tag{21}$$

A detailed derivation of formula (21) can be found in Section B. Although this approach is similar to that described in Ref. 33, the formula for the sheet resistance (21) differs from (11) obtained by Kumar and Kulkarni [33]. This difference is due to the number of edges intersecting any equipotential, viz., to find this number, we used a rigorous probabilistic derivation, while Kumar and Kulkarni [33] utilized an estimate  $(L_y\sqrt{n_{\rm E}})$ . It would be very tempting to simplify formula (21) by finding the exact value of the factor  $\beta$  in the relationship between the average length of a crack segment and the concentration of cracks (16). Unfortunately, only estimates are possible (see Appendix C). However, Figure 4 evidenced that (16) holds for the networks under consideration.

Note, the dependence of the sheet conductance on the fill fraction is linear, viz.,

$$G_{\square} = \frac{\sigma t f_{\rm F}}{2},\tag{22}$$

since  $f_F = n_E w \langle l \rangle$ . Accounting for (1),  $n_E w \langle l \rangle = 1 - T$ , hence,

$$T = 1 - \frac{2\rho}{tR_{\square}}. (23)$$

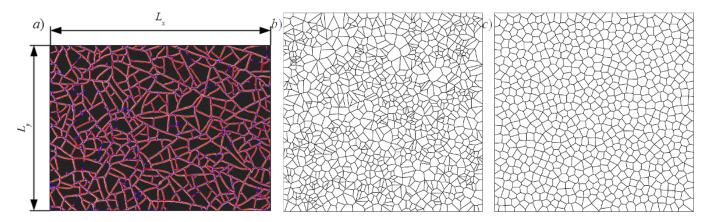


FIG. 2. Examples of the crack patterns. a) Sample 1, a real-world crack pattern (courtesy of A.S. Voronin) along with a corresponding network obtained using StructuralGT [46]. b) A computer-generated network produced using Voronoi tessellation based on randomly distributed points. c) A computer-generated network produced using Voronoi tessellation based on random hyperuniformly distributed points.

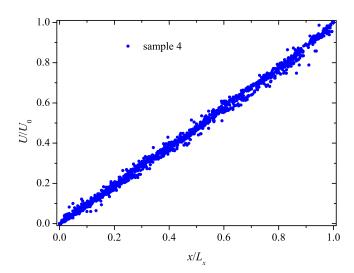


FIG. 3. Example of a potential distribution along a sample.

This relation resembles that obtained for a square mesh (7). The total mass of the metal deposited in the cracks is

$$m = n_{\rm E} \langle l \rangle w t \rho_m L_x L_y, \tag{24}$$

where  $\rho_m$  is the metal density.

# III. RESULTS

Figure 5 demonstrates the degree distribution in these 10 particular samples. In the box and whisker charts, here and below, the mean values are shown using markers, the 'box' presents the median, 25 and 75 percentiles, while the 'whiskers' indicate the minimal and maximal values. These distributions evidenced that T- and Y-shaped ( $\deg V = 3$ ) crack junctions dominate.  $\deg V = 1$  corresponds to both the internal nodes (dead ends) and to nodes on the boundaries (the intersections of cracks with image boundaries). A proportion

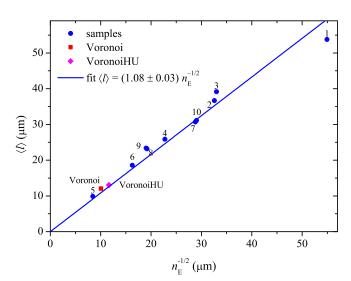


FIG. 4. Dependency of the mean length of crack segments on the number density of the cracks.

of dead ends is 0.15–0.3, while that of X-shaped ( $\deg V=4$ ) junctions is about 0.1. Here, we use the same notation to classify junctions as Gray et~al.~[48]. The proportions of nodes corresponding to  $\deg V=2$  and to  $\deg V=5$  are negligible. We suppose that vertices owning both  $\deg V=2$  and  $\deg V>4$  are artefacts rather than a reality, since the modest resolution of the images leads to only moderate accuracy of the image processing. By contrast, in networks produced using Voronoi tessellation, nodes with  $\deg V=1$  correspond solely to the intersections of edges with the domain boundaries. All internal nodes match  $\deg V=3$ . In general, in such artificial networks, the distribution of node degrees resembles that in real-world crack patterns.

Figure 6 demonstrates the distributions of crack orientations in the same real-world samples along with artificial computer-generated networks. These distributions evidenced that the cracks are approximately equiprobably oriented, i.e., the value of the order parameter (14) is close to 0. However,

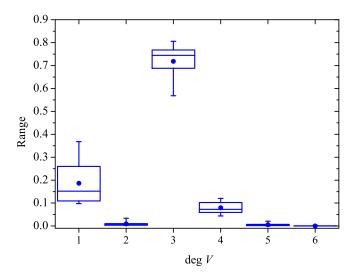


FIG. 5. Degree distribution in the 10 real-world samples.

the statistical variations are significant. Equiprobable distribution of crack orientations was also found for networks obtained using Voronoi tessellation. The values of the order parameter are presented in Table II. However, 'brickwork' patterns with two mutually perpendicular sets of parallel cracks can also be produced [49]. In that case, the orientations of the cracks have to obey a bimodal distribution.

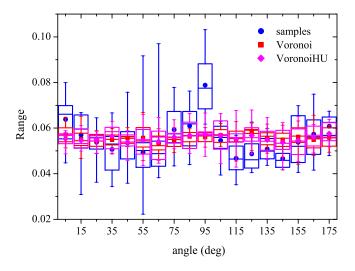


FIG. 6. Distribution of crack orientations in the particular realworld samples and in computer-generated networks produced using Voronoi tessellation.

Figure 7 demonstrates the distributions of angles between adjacent cracks in the same samples. These distributions evidenced that, in the real-world samples, cracks tend to join at right angles (T-shaped junctions). The maximum of the distribution is located near the angle  $90^{\circ}$  ( $\pi/2$  rad) (two right angles in each T-shaped junction); a less pronounces maximum located near  $180^{\circ}$  ( $\pi$  rad) corresponds to the straight angles in these T-shaped junctions. Such behavior is quite to be expected [50–52]. By contrast, networks obtained using

Voronoi tessellation demonstrate unimodal distribution with the maximum near  $120^{\circ}$  (2 rad), i.e., here, Y-shaped junctions dominate (Fig. 7). Note that, in the crack-template-based networks, the cracks are curved, while, in the corresponding networks produced using StructuralGT, the corresponding edges are straight. Consequently, the resulting distribution of angles between adjacent cracks is more diffuse in the vicinity of  $90^{\circ}$  ( $\pi/2$  rad) than it should be.

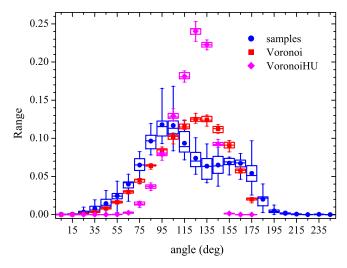


FIG. 7. Distribution of angles between adjacent cracks in the real-world samples and in the computer-generated networks produced using Voronoi tessellation.

Figure 8 demonstrates the distributions of normalized crack length in the same samples. Here,  $\langle l \rangle$  denotes the mean crack length. Comparison of the distributions evidenced that, in the real-world and in the computer-generated networks, the length distributions are similar and resemble a log-normal distribution.

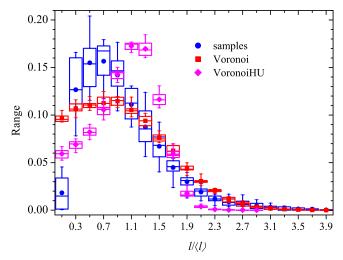


FIG. 8. Comparison of distribution of crack lengths in realworld samples and in computer-generated networks produced using Voronoi tessellation.

This preliminary analysis evidenced that Voronoi tessella-

tion produces networks, the topology which is close to the real crack-template-based networks while their geometries differ.

Tables II and III evidenced that the approach by Kumar and Kulkarni [33] significantly (1.5–2 times) overestimates the number of intersections of cracks with an equipotential line both for the real-world networks and for the computergenerated networks. Although the approach by Tarasevich *et al.* [35] is better (the overestimation is about 10% in the case of the real-world samples, while, in the case of the computergenerated networks, the prediction falls within the statistical error), the source of this overestimate needs to be identified.

Figure 4 suggests that, for random networks,  $\langle l \rangle \approx n_{\rm E}^{-1/2}$  since the factor  $\beta$  is close to unity. In this case, (B4) transforms in

$$G_{\square} = \frac{wt\sigma\sqrt{n_{\rm E}}}{2},\tag{25}$$

that differs from (11) by a factor of  $\pi/4$ .

Figure 9 plots the reduced electrical conductance of the samples against the square root of the number density of the cracks. The numbers near the markers indicate the numbers of the real-world samples. Since there was a difference in sheet resistance of the same sample computed using resistances in two directions, the averaged sheet resistance is presented for each sample. This difference arose due to the limited precision of the image processing caused by the quality of the photos. JAP2016 (markers and solid line) corresponds to prediction

$$\frac{G_{\square}}{wt\sigma} = \frac{2}{\pi}\sqrt{n_{\rm E}},\tag{26}$$

which is easily derived from (11). JAP2019 corresponds to the prediction (B4). Both predictions are close, although overestimate the electrical conductance. This deviation may arise due to differences between any particular sample and the imaginary averaged sample. For instance, for any real sample, the angular distribution can be far from the uniform distribution (Fig. 6). Besides, the potential drop along a sample is only *almost* linear rather than *strictly* linear (Fig. 3). In other words, a mean-field approach is based on an assumption that a sample is highly homogeneous and isotropic. This assumption is hardly exact for real-world samples, however, it is expected to be much better for our computer-generated samples, especially for hyperuniform ones.

Figure 10 plots the reduced electrical conductance of the computer-generated networks against the square root of the number density of the cracks. It is noticeable that, for hyperuniform samples, prediction (B4) is excellent. This suggests that heterogeneity of any particular sample may be a reasonable cause for both (11) and (B4) to overestimate the electrical conductance. Nevertheless, homogeneity of samples (e.g., transparent heaters) is a natural requirement. Thus, the prediction (B4) can be considered as a theoretical limit of the on the maximum electrical conductance that a highly uniform random network can reach.

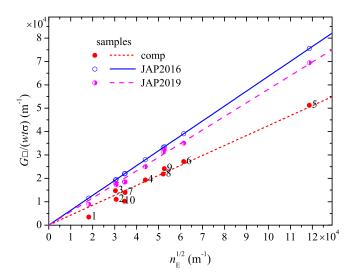


FIG. 9. Reduced conductance vs square root of the number density of cracks. JAP2016 corresponds to prediction (26), JAP2019 corresponds to prediction (B4). Dashed lines correspond to least squares fits. Numbers near the markers indicate the number of the sample.

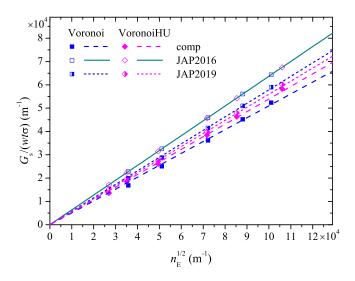


FIG. 10. Reduced conductance vs square root of the number density of cracks. JAP2016 corresponds to prediction (26), JAP2019 corresponds to prediction (B4). Dashed lines correspond to least squares fits.

# IV. CONCLUSION

We performed image processing and analysis of 10 photos of crack-template based TCFs. The analysis evidenced that (i) the angle distribution is almost equiprobable; however, the statistical errors are significant, i.e., the properties of a particular sample may differ significantly from the average values (Fig. 6); (ii) secondary cracks tends to be perpendicular to the primary ones, i.e., T-shaped connections of cracks are dominant; as a result, the typical angles between adjacent cracks are about 90° and 180° (Fig. 7); (iii) the length distribution of crack segments resembles a log-normal distribution (Fig. 8);

TABLE II. Number of intersections in real-world samples.

Smp	S	s Simulation		Eq.	(12)	Eq. (15)	
		$\boldsymbol{x}$	y	X	у	X	у
1	$-0.01 \pm 0.03$	$13.08 \pm 0.12$	$19.35 \pm 0.32$	21.4886	31.6446	14.0815	20.7367
2	$-0.047 \pm 0.021$	$19.35 \pm 0.12$	$28.16 \pm 0.15$	29.9026	39.8962	21.4941	28.6775
3	$0.007 \pm 0.017$	$25.81 \pm 0.18$	$35.18 \pm 0.20$	37.5066	49.9112	28.2236	37.5579
4	$0.012 \pm 0.017$	$35.42 \pm 0.17$	$35.78 \pm 0.19$	50.8029	50.9026	38.8360	38.9122
5	$-0.079 \pm 0.023$	$16.88 \pm 0.14$	$28.40 \pm 0.21$	25.4009	37.0853	18.7475	27.3714
6	$-0.010 \pm 0.022$	$17.02 \pm 0.12$	$29.21 \pm 0.19$	25.6971	42.2226	18.6698	30.6761
7	$-0.018 \pm 0.030$	$13.38 \pm 0.09$	$18.56 \pm 0.13$	20.5013	29.5103	13.9044	20.0145
8	$0.072 \pm 0.018$	$25.49 \pm 0.15$	$32.90 \pm 0.24$	33.3887	49.5977	25.6134	38.0478
9	$0.046 \pm 0.018$	$25.17 \pm 0.16$	$34.30 \pm 0.24$	33.1937	51.2447	25.9509	40.0632
10	$0.006 \pm 0.024$	$16.63 \pm 0.14$	$23.98 \pm 0.26$	26.1745	38.4344	17.8347	26.1883

TABLE III. Number of intersections in computer-generated samples.

Smp	Simu	lation	Eq. (12)	Eq. (15)		
	x	у				
Voronoi						
1	$39.59 \pm 0.66$	$39.47 \pm 0.67$	54.2679	39.5815		
2	$39.44 \pm 0.64$	$40.63 \pm 0.57$	54.3047	39.9485		
3	$40.03 \pm 0.79$	$39.75 \pm 0.62$	54.3967	39.7988		
4	$38.81 \pm 0.68$	$39.69 \pm 0.65$	54.3323	39.4767		
5	$38.78 \pm 0.68$	$39.16 \pm 0.87$	54.4243	39.5114		
6	$39.66 \pm 0.80$	$40.13 \pm 0.75$	54.4151	39.5292		
7	$40.06 \pm 0.81$	$40.34 \pm 0.72$	54.3691	39.8669		
8	$39.94 \pm 0.72$	$40.03 \pm 0.68$	54.3415	39.6991		
9	$39.19 \pm 0.47$	$39.84 \pm 0.73$	54.3599	39.6767		
10	$38.69 \pm 0.78$	$40.06\pm0.65$	54.3783	39.6188		
		VoronoiHU				
1	$31.50 \pm 0.44$	$31.75 \pm 0.40$	44.5870	31.3162		
2	$31.41 \pm 0.45$	$31.28 \pm 0.38$	44.3959	31.2962		
3	$31.00 \pm 0.44$	$31.75 \pm 0.48$	44.7661	31.4797		
4	$31.53 \pm 0.45$	$31.03 \pm 0.44$	45.0222	31.6740		
5	$31.03 \pm 0.37$	$30.19 \pm 0.46$	44.5197	31.3243		
6	$31.19 \pm 0.35$	$32.03 \pm 0.40$	44.8665	31.6408		
7	$31.60 \pm 0.50$	$32.09 \pm 0.43$	44.9110	31.5567		
8	$31.66 \pm 0.41$	$31.31 \pm 0.49$	44.7661	31.5408		
9	$31.34 \pm 0.51$	$32.06 \pm 0.45$	44.6542	31.3690		
10	$31.81 \pm 0.39$	$31.00 \pm 0.47$	44.8553	31.5963		

(iv) the average length of crack segments is inversely proportional to the square root of the number density of the cracks (Fig. 4).

We analyzed computer-generated networks obtained using kinds of Voronoi tessellation. In the first case, the generators (points) were randomly distributed within a square domain. In the second case, discs were deposited in the square domain using random sequential adsorption. The centers of these discs were used as random hyperuniformly distributed points to perform the Voronoi tessellation. The analysis evidenced that, for both kinds of network, (i) the angle distribution is equiprobable (Fig. 6); (ii) Y-shaped connections of cracks dominate; as a result, the typical angles between adjacent cracks are about 120° (Fig. 7); (iii) the length distribution of the crack segments resembles a log-normal distribution (Fig. 8); (iv) the average length of the crack segments is inversely proportional

to the square root of the number density of the cracks (Fig. 4).

Our computations suggest that (i) the potential drop along the samples is almost linear (Fig. 3); (ii) the theoretically predicted [33, 35] proportionality of the electrical conductance to the square root of the number density of cracks is correct (Fig. 9); however, both approaches overestimate the electrical conductance. We suppose, there are two main reason for this overestimation. Both approaches are based largely on the assumptions that (i) the voltage drop is strictly linear and (ii) the angle distribution is strictly equiprobable. In fact, both of these requirements are met only approximately. Moreover, approach by Kumar and Kulkarni [33] significantly overestimate the number of cracks intersecting an equipotential line (see Table II and Table III).

### **ACKNOWLEDGMENTS**

We acknowledge funding from the Russian Science Foundation, Grant No. 23-21-00074. We thank A.S. Voronin for the unpublished photos of crack templates (denoted as sample 1 and sample 2 in this work).

#### DATA AVAILABILITY STATEMENT

The data that support the findings of this study are available from the corresponding author upon reasonable request.

# Appendix A: Electrical conductance of variable width wire

Let there be a junction-free random conductive network produced using a crack pattern. Consider one conductive segment between two nearest points of intersection of the cracks. We will assume that this segment is straight and has a length l. Let us direct axis x along this conductive segment. We will consider the thickness of the conductor to be a constant t, while the width of the conductor is variable w(x).

Let the resistivity of the material filling the cracks be equal to  $\rho$ . Then the resistance of the segment under consideration

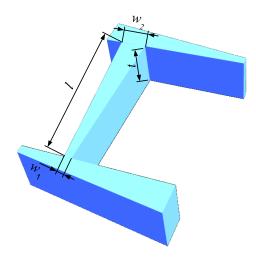


FIG. 11. Sizes of a conductive segment.

is equal to

$$R = \frac{\rho}{t} \int_{0}^{l} \frac{\mathrm{d}x}{w(x)}.$$
 (A1)

Consider the simplest situation, when the width of the conductor changes linearly from  $w_1$  to  $w_2$  ( $w_1 < w_2$ )

$$w(x) = w_1 + \frac{w_2 - w_1}{l}x.$$
 (A2)

Hence,

$$R = \frac{\rho l}{t} \int_{0}^{l} \frac{\mathrm{d}x}{w_1 l + (w_2 - w_1)x} = \frac{\rho l}{t(w_2 - w_1)} \ln \frac{w_2}{w_1}.$$
 (A3)

The electrical conductance of this segment is equal to

$$G = \frac{\sigma t}{l} \frac{w_2 - w_1}{\ln w_2 - \ln w_1},$$
 (A4)

where  $\sigma$  is the electrical conductivity of the material, while the second factor is the logarithmic mean. Introducing a notation  $w_2 = \langle w \rangle + \Delta$ ,  $w_1 = \langle w \rangle - \Delta$ , we get

$$\frac{w_2 - w_1}{\ln w_2 - \ln w_1} = \frac{2\Delta}{\ln \frac{\langle w \rangle + \Delta}{\langle w \rangle - \Delta}}.$$
 (A5)

When  $\Delta \ll \langle w \rangle$ ,

$$\ln \frac{\langle w \rangle + \Delta}{\langle w \rangle - \Delta} \approx 2 \frac{\Delta}{\langle w \rangle}, \tag{A6}$$

hence,

$$\frac{w_2 - w_1}{\ln w_2 - \ln w_1} \approx \langle w \rangle. \tag{A7}$$

Thus,

$$G \approx \frac{\sigma t \langle w \rangle}{l}, \quad R \approx \frac{\rho l}{t \langle w \rangle}.$$
 (A8)

# Appendix B: Electrical conductance of a crack-template based random network

Here, we reproduce with minor changes derivations presented in Tarasevich *et al.* [35]. These changes are intended to adapt the consideration of a random resistor network produced by randomly placed nanowires to the case of crack-template-based networks. Consider a network of size  $L_x \times L_y$ . When the total number of edges (cracks) is  $N_E$ , the number density of edges is

$$n_{\rm E} = \frac{N_{\rm E}}{L_{\rm x}L_{\rm y}}.\tag{B1}$$

Let l be the length of a particular edge, i.e., the length of the crack between the two nearest crossing points (nodes). The resistance of this edge is described by (19).

Let a potential difference,  $U_0$ , be applied to the opposite boundaries of the film along the x direction. Since, in devices such as transparent heaters, solar cells, touch screens, etc., any typical face size (a smallest region of the film bounded by cracks) is much less than the linear film size, a potential drop along the sample is almost linear (Fig. 3). The potential difference between the ends of an i-th crack, oriented at angle  $\alpha$  with respect to the external electrostatic field, is

$$\frac{U_0 l \cos \alpha}{L_x}$$
.

Hence, the electric current in this filled crack is

$$i(\alpha) = \frac{U_0 l \cos \alpha}{L_x R} = \frac{U_0 w t \cos \alpha}{L_x \rho}.$$
 (B2)

Consider a line, which is perpendicular to the external electrostatic field. A crack, that is oriented with respect to this field at angle  $\alpha$ , intersects this line, if its origin is located at a distance not exceeding  $l\cos\alpha$  from the line. The number of appropriate edges (crack segments) is  $n_{\rm E}lL_{\rm y}\cos\alpha$ , while the overall electrical current in all such filled cracks is

$$\frac{U_0 n_{\rm E} lwt L_{\rm y} \cos^2 \alpha}{\rho L_{\rm x}}.$$

The total electric current is

$$I = \frac{1}{\pi} \int_{l_{\min} - \pi/2}^{l_{\max}} \int_{-\pi/2}^{\pi/2} \frac{U_0 n_{\text{E}} w t L_y}{\rho L_x} f(l) l \cos^2 \alpha \, d\alpha \, dl$$

$$= \frac{U_0 n_{\text{E}} \langle l \rangle w t L_y}{2\rho L_x}. \quad (B3)$$

Since the all crack orientations are equiprobable and  $\alpha \in [-\pi/2,\pi/2]$ , the probability density function (PDF) of the angle orientations is  $\pi^{-1}$ . f(l) is the PDF, which describes the distribution of the cracks' length with the distribution's support  $l \in [l_{\min}, l_{\max}]$ .  $\langle \cdot \rangle$  denotes the mean value. Therefore, the electrical sheet conductance is

$$G_{\square} = \frac{\sigma n_{\rm E} \langle l \rangle wt}{2},\tag{B4}$$

where  $\sigma = \rho^{-1}$  is the electrical conductivity of the metal. In contrast with (26), the sheet conductance depends not only on the number density of the cracks, but also on the average crack length. However, accounting for relation (16), the dependency on the average crack length can be eliminated, and as a result the sheet conductance is expected to be dependent on the number density of the cracks as  $\sqrt{n_{\rm E}}$ .

# Appendix C: Relationship between the average length of a crack segment and the concentration of cracks

Let a crack network split the sample into F faces (cells). In the case of computer-generated networks based on the Voronoi tessellation, this means using F points for its generation. Let E be the number of edges in this network, and let  $\langle l \rangle$  be the average length of one edge. When the sample has dimensions  $L_x \times L_y$ , the average area of one face is

$$\langle A_{\rm F} \rangle = \frac{L_x L_y}{F},$$
 (C1)

while the number density of the edges is defined by (B1). Obviously,

$$\sum_{i=1}^{V} \deg V_i = 2E \tag{C2}$$

or

$$\frac{1}{V} \sum_{i=1}^{V} \deg V_i = \frac{2E}{V}, \quad \langle \deg V \rangle = \frac{2E}{V}, \quad V = \frac{2E}{\langle \deg V \rangle}. \quad (C3)$$

According to Euler's formula for planar graphs (networks) V - E + F = 2, where V is the number of vertices, while the number of faces, F, accounts for the outer, infinitely large face. Since the outer face is out of our interest, F = E - V + 1. Therefore,

$$F = \left(1 - \frac{2}{\langle \deg V \rangle}\right) E + 1. \tag{C4}$$

Note, that if the number of faces is large  $(F \gg 1)$ , then  $E - V \approx F$ . Let's move from the number of edges, E, to their number density (B1) and the average face area (C1)

$$\langle A_{\rm F} \rangle^{-1} = \left( 1 - \frac{2}{\langle \deg V \rangle} \right) n_{\rm E} + \frac{1}{L_{\rm x} L_{\rm y}}.$$
 (C5)

When  $E \gg 1$ , which is ensured in the case of crack patterns,

$$\langle A_{\rm F} \rangle^{-1} \approx \left( 1 - \frac{2}{\langle \deg V \rangle} \right) n_{\rm E}.$$
 (C6)

Since, in the case of computer-generated networks based on the Voronoi tessellation,  $\langle \deg V \rangle \approx 3$ ,

$$\langle A_{\rm F} \rangle^{-1} \approx \frac{n_{\rm E}}{3}.$$
 (C7)

A circle has the smallest perimeter among all figures of the same area, hence, the perimeter of one face is limited by the value of the circumference, determined as follows. Since, for a circle,  $\langle A_{\rm F} \rangle = \pi r^2$ , then

$$r = \sqrt{\frac{\langle A_{\rm F} \rangle}{\pi}}.$$
 (C8)

Whereas the circumference is  $C = 2\pi r$ , then

$$\langle C \rangle = 2\pi \sqrt{\frac{\langle A_{\rm F} \rangle}{\pi}} = 2\sqrt{\langle A_{\rm F} \rangle \pi}.$$
 (C9)

The perimeter of any face is obviously greater than the circumference of a circle of the same area.

Since each edge belongs to two faces, the total length of all edges,  $\langle l \rangle E$ , is greater or equal to  $F \langle C \rangle / 2$ , i.e.,  $\langle l \rangle E \geqslant F \sqrt{\pi \langle A_F \rangle}$ . Using the approximate value of the average face area (C7),

$$\langle l \rangle \gtrsim \sqrt{\frac{\pi}{3n_{\rm E}}} \approx 1.023 n_{\rm E}^{-1/2}.$$
 (C10)

Hence,

$$n_{\rm E}\langle l\rangle \gtrapprox \sqrt{\frac{\pi n_{\rm E}}{3}}.$$
 (C11)

If the domain is divided into identical square cells, then the number of such cells (faces) is equal to

$$F = \frac{L_x L_y}{\langle l \rangle^2}.$$
 (C12)

The number of edges equals

$$E = 2F = \frac{2L_x L_y}{\langle l \rangle^2}.$$
 (C13)

The number density of edges is equal to

$$n_{\rm E} = \frac{2}{\langle l \rangle^2}.\tag{C14}$$

Hence, the average edge length depends on the number density of the cracks as follows

$$\langle l \rangle = \sqrt{\frac{2}{n_{\rm E}}}.$$
 (C15)

The total edge length is

$$\frac{2\langle l\rangle L_x L_y}{\langle l\rangle^2}.$$
 (C16)

The area of one face (cell) equals

$$A_F = \langle l \rangle^2. \tag{C17}$$

If the partitioning of the area is made in the form of a brickwork pattern, then the degrees of the vertices are 3, and the angles between the edges are straight, which resembles the properties of crack networks. The number of faces (cells) is equal to

$$F = \frac{L_x L_y}{2\langle I \rangle^2}.$$
 (C18)

The number of edges equals

$$n_{\rm E} = \frac{3}{2\langle l \rangle^2}.\tag{C20}$$

The average edge length depends on the number density of edges as follows

$$\langle l \rangle = \sqrt{\frac{3}{2n_{\rm E}}} \approx 1.225 n_{\rm E}^{-1/2}.$$
 (C21)

Hence,

$$n_{\rm E}\langle l\rangle = \sqrt{\frac{3n_{\rm E}}{2}}.$$
 (C22)

- $E = 3F = \frac{3L_x L_y}{2\langle l \rangle^2}.$  (C19)
- Yanhua Liu, Su Shen, Jin Hu, and Linsen Chen, "Embedded Ag mesh electrodes for polymer dispersed liquid crystal devices on flexible substrate," Opt. Express 24, 25774 (2016).
- [2] Yu Han, Jie Lin, Yuxuan Liu, Hao Fu, Yuan Ma, Peng Jin, and Jiubin Tan, "Crackle template based metallic mesh with highly homogeneous light transmission for high-performance transparent EMI shielding," Sci. Rep. 6, 25601 (2016).
- [3] Su Shen, Shi-Yu Chen, Dong-Yu Zhang, and Yan-Hua Liu, "High-performance composite Ag—Ni mesh based flexible transparent conductive film as multifunctional devices," Opt. Express 26, 27545 (2018).
- [4] Zhou-ying Jiang, Wenbin Huang, Lin-sen Chen, and Yan-hua Liu, "Ultrathin, lightweight, and freestanding metallic mesh for transparent electromagnetic interference shielding," Opt. Express 27, 24194 (2019).
- [5] Naitao Song, Qiao Sun, Su Xu, Dongzhi Shan, Yang Tang, Xiaoxi Tian, Nianxi Xu, and Jinsong Gao, "Ultra-wide-band optically transparent anti-diffraction metamaterial absorber with a thiessen-polygon metal-mesh shielding layer," Photonics Res. (2023), 10.1364/prj.486613.
- [6] Hongke Li, Denghua Zi, Xiaoyang Zhu, Houchao Zhang, Yuping Tai, Rui Wang, Luanfa Sun, Youchao Zhang, Wensong Ge, Youqi Huang, Gang Liu, Wenchao Yang, Jianjun Yang, and Hongbo Lan, "Electric field driven printing of repeatable random metal meshes for flexible transparent electrodes," Opt. Laser Technol. 157, 108730 (2023).
- [7] Young D. Suh, Jinhyeong Kwon, Jinhwan Lee, Habeom Lee, Seongmin Jeong, Dongkwan Kim, Hyunmin Cho, Junyeob Yeo, and Seung Hwan Ko, "Maskless fabrication of highly robust, flexible transparent Cu conductor by random crack network assisted Cu nanoparticle patterning and laser sintering," Adv. Electron. Mater. 2, 1600277 (2016).
- [8] Young D. Suh, Sukjoon Hong, Jinhwan Lee, Habeom Lee, Seongmin Jung, Jinhyeong Kwon, Hyunjin Moon, Phillip Won, Jaeho Shin, Junyeob Yeo, and Seung Hwan Ko, "Random nanocrack, assisted metal nanowire-bundled network fabrication for a highly flexible and transparent conductor," RSC Adv. 6, 57434–57440 (2016).
- [9] Jinwook Jung, Hyunmin Cho, Seok Hwan Choi, Dongkwan Kim, Jinhyeong Kwon, Jaeho Shin, Sukjoon Hong, Hyeonseok Kim, Yeosang Yoon, Jinwoo Lee, Daeho Lee, Young D. Suh, and Seung Hwan Ko, "Moiré-free imperceptible and flexible random metal grid electrodes with large figure-of-merit by

- photonic sintering control of copper nanoparticles," ACS Appl. Mater. Interfaces **11**, 15773–15780 (2019).
- [10] Sunil Walia, Indrajit Mondal, and Giridhar U. Kulkarni, "Patterned Cu-mesh-based transparent and wearable touch panel for tactile, proximity, pressure, and temperature sensing," ACS Appl. Electron. Mater. 1, 1597–1604 (2019).
- [11] Anna M. Melnychenko and Robert Kudrawiec, "Crack-templated wire-like semitransparent electrodes with unique irregular patterns," ACS Omega 7, 39181–39186 (2022).
- [12] Hock Beng Lee, Won-Yong Jin, Manoj Mayaji Ovhal, Neetesh Kumar, and Jae-Wook Kang, "Flexible transparent conducting electrodes based on metal meshes for organic optoelectronic device applications: a review," J. Mater. Chem. C 7, 1087–1110 (2019).
- [13] K. D. M. Rao and Giridhar U. Kulkarni, "A highly crystalline single Au wire network as a high temperature transparent heater," Nanoscale 6, 5645 (2014).
- [14] Bing Han, Ke Pei, Yuanlin Huang, Xiaojian Zhang, Qikun Rong, Qinggeng Lin, Yangfei Guo, Tianyi Sun, Chuanfei Guo, David Carnahan, Michael Giersig, Yang Wang, Jinwei Gao, Zhifeng Ren, and Krzysztof Kempa, "Uniform self-forming metallic network as a high-performance transparent conductive electrode," Adv. Mater. 26, 873–877 (2014).
- [15] K. D. M. Rao, Christoph Hunger, Ritu Gupta, Giridhar U. Kulkarni, and Mukundan Thelakkat, "A cracked polymer templated metal network as a transparent conducting electrode for ITO-free organic solar cells," Phys. Chem. Chem. Phys. 16, 15107–15110 (2014).
- [16] Ke Pei, Zongrong Wang, Xiaochen Ren, Zhichao Zhang, Boyu Peng, and Paddy K. L. Chan, "Fully transparent organic transistors with junction-free metallic network electrodes," Appl. Phys. Lett. 107, 033302 (2015).
- [17] Qiang Peng, Songru Li, Bing Han, Qikun Rong, Xubing Lu, Qianming Wang, Min Zeng, Guofu Zhou, Jun-Ming Liu, Krzysztof Kempa, and Jinwei Gao, "Colossal figure of merit in transparent-conducting metallic ribbon networks," Adv. Mater. Technol. 1, 1600095 (2016).
- [18] A. S. Voronin, F. S. Ivanchenko, M. M. Simunin, A. V. Shiverskiy, Aleksandrovsky, I. V. Nemtsev, Y. V. Fadeev, D. V. Karpova, and S. V. Khartov, "High performance hybrid rGO/Ag quasi-periodic mesh transparent electrodes for flexible electrochromic devices," Appl. Surf. Sci. 364, 931–937 (2016).
- [19] A. S. Voronin, M. M. Simunin, Yu. V. Fadeev, F. S. Ivanchenko,

- D. V. Karpova, I. A. Tambasov, and S. V. Khartov, "Technological basis of the formation of micromesh transparent electrodes by means of a self-organized template and the study of their properties," Tech. Phys. Lett. **45**, 366–369 (2019).
- [20] A. S. Voronin, Yu. V. Fadeev, I. V. Govorun, A. S. Voloshin, I. A. Tambasov, M. M. Simunin, and S. V. Khartov, "A transparent radio frequency shielding coating obtained using a selforganized template," Tech. Phys. Lett. 47, 259–262 (2021).
- [21] A. S. Voronin, Y. V. Fadeev, I. V. Govorun, I. V. Podshivalov, M. M. Simunin, I. A. Tambasov, D. V. Karpova, T. E. Smolyarova, A. V. Lukyanenko, A. A. Karacharov, I. V. Nemtsev, and S. V. Khartov, "Cu–Ag and Ni–Ag meshes based on cracked template as efficient transparent electromagnetic shielding coating with excellent mechanical performance," J. Mater. Sci. 56, 14741–14762 (2021).
- [22] A. S. Voronin, Y. V. Fadeev, F. S. Ivanchenko, S. S. Dobrosmyslov, M. O. Makeev, P. A. Mikhalev, A. S. Osipkov, I. A. Damaratsky, D. S. Ryzhenko, G. Y. Yurkov, M. M. Simunin, M. N. Volochaev, I. A. Tambasov, S. V. Nedelin, N. A. Zolotovsky, D. D. Bainov, and S. V. Khartov, "Original concept of cracked template with controlled peeling of the cells perimeter for high performance transparent EMI shielding films," Surf. Interfaces 38, 102793 (2023).
- [23] Seoin Kang, Vinaya Kumar Arepalli, Eunyeong Yang, Sangyeob Lee, Jung-Sub Wi, Jae Ho Yun, Soomin Song, Kihwan Kim, Young-Joo Eo, Jun-Sik Cho, Jihye Gwak, and Choong-Heui Chung, "High performance and flexible electrodeposited silver mesh transparent conducting electrodes based on a self-cracking template," Electron. Mater. Lett. 18, 440–446 (2022).
- [24] Kin Wai Cheuk, Ke Pei, and Paddy K. L. Chan, "Degradation mechanism of a junction-free transparent silver network electrode," RSC Adv. 6, 73769–73775 (2016).
- [25] Anton S. Voronin, Yurii V. Fadeev, Mstislav O. Makeev, Pavel A. Mikhalev, Alexey S. Osipkov, Alexander S. Provatorov, Dmitriy S. Ryzhenko, Gleb Y. Yurkov, Mikhail M. Simunin, Darina V. Karpova, Anna V. Lukyanenko, Dieter Kokh, Dashi D. Bainov, Igor A. Tambasov, Sergey V. Nedelin, Nikita A. Zolotovsky, and Stanislav V. Khartov, "Low cost embedded copper mesh based on cracked template for highly durability transparent EMI shielding films," Materials 15, 1449 (2022).
- [26] Sunil Walia, Ashutosh K. Singh, Veena S. G. Rao, Suryasarathi Bose, and Giridhar U. Kulkarni, "Metal mesh-based transparent electrodes as high-performance EMI shields," Bull. Mater. Sci. 43, 187 (2020).
- [27] Ping Liu, Bing Huang, Lei Peng, Liming Liu, Qingguo Gao, and Yuehui Wang, "A crack templated copper network film as a transparent conductive film and its application in organic light-emitting diode," Sci. Rep. 12, 20494 (2022).
- [28] Indrajit Mondal, Gaurav Bahuguna, Mukhesh K. Ganesha, Mohit Verma, Ritu Gupta, Ashutosh K. Singh, and Giridhar U. Kulkarni, "Scalable fabrication of scratch-proof transparent Al/F-SnO<sub>2</sub> hybrid electrodes with unusual thermal and environmental stability," ACS Appl. Mater. Interfaces 12, 54203–54211 (2020).
- [29] Remya K. Govind, Indrajit Mondal, Kaushik Baishya, Mukhesh K. Ganesha, Sunil Walia, Ashutosh K. Singh, and Giridhar U. Kulkarni, "Large-area fabrication of high performing, flexible, transparent conducting electrodes using screen printing and spray coating techniques," Adv. Mater. Technol. 7, 2101120 (2022).
- [30] D. S. Ghosh, T. L. Chen, and V. Pruneri, "High figure-of-merit ultrathin metal transparent electrodes incorporating a conduc-

- tive grid," Appl. Phys. Lett. 96, 041109 (2010).
- [31] Julian Schneider, Patrik Rohner, Deepankur Thureja, Martin Schmid, Patrick Galliker, and Dimos Poulikakos, "Electrohydrodynamic NanoDrip printing of high aspect ratio metal grid transparent electrodes," Adv. Funct. Mater. 26, 833–840 (2016).
- [32] Christopher P. Muzzillo, Matthew O. Reese, and Lorelle M. Mansfield, "Fundamentals of using cracked film lithography to pattern transparent conductive metal grids for photovoltaics," Langmuir 36, 4630–4636 (2020).
- [33] Ankush Kumar and G. U. Kulkarni, "Evaluating conducting network based transparent electrodes from geometrical considerations," J. Appl. Phys. 119, 015102 (2016).
- [34] Ankush Kumar, N. S. Vidhyadhiraja, and Giridhar U. Kulkarni, "Current distribution in conducting nanowire networks," J. Appl. Phys. 122, 045101 (2017).
- [35] Yuri Yu. Tarasevich, Irina V. Vodolazskaya, Andrei V. Eserkepov, and Renat K. Akhunzhanov, "Electrical conductance of two-dimensional composites with embedded rodlike fillers: An analytical consideration and comparison of two computational approaches," J. Appl. Phys. 125, 134902 (2019).
- [36] D. Frenkel and R. Eppenga, "Evidence for algebraic orientational order in a two-dimensional hard-core nematic," Phys. Rev. A 31, 1776–1787 (1985).
- [37] Sabine Le Roux, Farid Medjedoub, Gilles Dour, and Farhad Rézaï-Aria, "Image analysis of microscopic crack patterns applied to thermal fatigue heat-checking of high temperature tool steels," Micron 44, 347–358 (2013).
- [38] Lucas Goehring, Akio Nakahara, Tapati Dutta, So Kitsunezaki, and Sujata Tarafdar, *Desiccation Cracks and Their Patterns* (Wiley-VCH Verlag GmbH, 2015) p. 368.
- [39] Zijing Zeng, Changhong Wang, and Jinwei Gao, "Numerical simulation and optimization of metallic network for highly efficient transparent conductive films," J. Appl. Phys. 127, 065104 (2020).
- [40] Jaeuk Kim and Thomas M. Truskett, "Geometric model of crack-templated networks for transparent conductive films," Appl. Phys. Lett. 120, 211108 (2022).
- [41] K. Esteki, D. Curic, H. G. Manning, E. Sheerin, M. S. Ferreira, J. J. Boland, and C. G. Rocha, "Thermo-electro-optical properties of seamless metallic nanowire networks for transparent conductor applications," Nanoscale 15, 10394–10411 (2023).
- [42] A. Roy, R. A. I. Haque, A. J. Mitra, S. Tarafdar, and T. Dutta, "Combinatorial topology and geometry of fracture networks," Phys. Rev. E 105, 034801 (2022).
- [43] The unpublished photos were kindly provided by A.S. Voronin who is one the authors of that article[21].
- [44] Zhike Xian, Bing Han, Songru Li, Chaobin Yang, Sujuan Wu, Xubing Lu, Xingsen Gao, Min Zeng, Qianming Wang, Pengfei Bai, Michael J. Naughton, Guofu Zhou, Jun-Ming Liu, Krzysztof Kempa, and Jinwei Gao, "A practical ITO replacement strategy: Sputtering-free processing of a metallic nanonetwork," Adv. Mater. Technol. 2, 1700061 (2017).
- [45] Jinwei Gao, Zhike Xian, Guofu Zhou, Jun-Ming Liu, and Krzysztof Kempa, "Nature-inspired metallic networks for transparent electrodes," Adv. Funct. Mater. 28, 1705023 (2018).
- [46] Drew Vecchio, Samuel Mahler, Mark D. Hammig, and Nicholas A. Kotov, "StructuralGT," github (2021).
- [47] Gaël Guennebaud, Benoît Jacob, et al., "Eigen v3," https://eigen.tuxfamily.org/ (2010).
- [48] N. H. Gray, J. B. Anderson, J. D. Devine, and J. M. Kwasnik, "Topological properties of random crack networks," J. Int. Ass. Math. Geol. 8, 617–626 (1976).
- [49] Shuyao Xie, Teng Li, Zijie Xu, Yanan Wang, Xiangyang Liu, and Wenxi Guo, "A high-response transparent heater based on

- a CuS nanosheet film with superior mechanical flexibility and chemical stability," Nanoscale  ${f 10},\,6531-6538$  (2018).
- [50] S. Bohn, L. Pauchard, and Y. Couder, "Hierarchical crack pattern as formed by successive domain divisions." Phys. Rev. E 71, 046214 (2005).
- [51] S. Bohn, J. Platkiewicz, B. Andreotti, M. Adda-Bedia, and
- Y. Couder, "Hierarchical crack pattern as formed by successive domain divisions. II. From disordered to deterministic behavior," Phys. Rev. E **71**, 046215 (2005).
- [52] Ankush Kumar and G. U. Kulkarni, "Time evolution and spatial hierarchy of crack patterns," Langmuir 37, 13141–13147 (2021).